Material Quality Characterization of CdZnTe Substrates for HgCdTe Epitaxy

G.A. CARINI,[1,2,8] C. ARNONE,[2] A.E. BOLOTNIKOV,[1] G.S. CAMARDA,[1] R. DE WAMES,[3] J.H. DINAN,[4] J.K. MARKUNAS,[4] B. RAGHOTHAMACHAR,[5] S. SIVANANTHAN,[6] R. SMITH,[7] J. ZHAO,[6] Z. ZHONG,[7] and R.B. JAMES[1]

1.—Brookhaven National Laboratory, Upton, NY 11973. 2.—Department of Electrical Engineering, University of Palermo, 90128 Palermo, Italy. 3.—Electro-Optics Center, Penn State University, Freeport, PA 16629. 4.—US Army RDECOM CERDEC NVESD, Ft. Belvoir, VA 22060. 5.—Department of Materials Sci. & Eng., Stony Brook University, Stony Brook, NY 11794. 6—Microphysics Laboratory, University of Illinois at Chicago, Chicago, IL 60607. 7.—National Synchrotron Light Source, BNL, Upton, NY 11973. 8.—E-mail: carini@bnl.gov

$Cd_{1-x}Zn_xTe$ (CZT) substrates were studied to investigate their bulk and surface properties. Imperfections in CZT substrates affect the quality of $Hg_{1-x}Cd_xTe$ (MCT) epilayers deposited on them and play a role in limiting the performance of infrared (IR) focal plane arrays. CZT wafers were studied to investigate their bulk and surface properties. Transmission and surface x-ray diffraction techniques, utilizing both a conventional closed-tube x-ray source as well as a synchrotron radiation source, and IR transmission microspectroscopy, were used for bulk and surface investigation. Synchrotron radiation offers the capability to combine good spatial resolution and shorter exposure times than conventional x-ray sources, which allows for high-resolution mapping of relatively large areas in an acceptable amount of time. Information on the location of grain boundaries and precipitates was also obtained. The ultimate goal of this work is to understand the defects in CZT substrates and their effects on the performance and uniformity of MCT epilayers and then to apply this understanding to produce better infrared detectors.

Key words: X-ray diffraction (XRD), rocking curve, x-ray topography, CdZnTe substrate, HgCdTe, Fourier transform infrared spectrometry (FTIR)

INTRODUCTION

$Hg_{1-x}Cd_xTe$ (MCT) is the leading material for infrared radiation detectors, and $Cd_{1-x}Zn_xTe$ (CZT) is the substrate of choice for high-quality MCT epilayers due to its lattice matching properties. More recently, heteroepitaxy of CdTe and CZT has been developed on Si and Ge as an alternative approach in order to reduce the cost of substrate production. Though more expensive, CZT is still the most widely used substrate due to its good compatibility with MCT epilayers. The current generation of devices requires fabrication processes with good versatility and quality for which molecular beam epitaxy (MBE) is best suited. Because the (211)B face was found to be the preferred orientation for MBE growth,[1] the quality of the MCT epilayers has vastly improved. Nevertheless, structural perfection of CZT crystals continues to be a major issue for the production of high-yield MCT devices. Defects propagating into the epilayer from the substrate are detrimental to detector performance,[2] and there is a significant need to better understand correlations between the substrate and epilayer properties.

In this paper, we present preliminary results of studies on CZT substrates. A series of techniques using synchrotron radiation was applied to investigate the bulk and surface properties. The low divergence and high brightness of the photon beam permit detailed microscale characterization, yielding high-resolution maps in areas of few square centimeters in size within a reasonable amount of time.

(Received November 23, 2005; accepted February 1, 2006)

Moreover, achieving detailed characterization on the spatial scale of the pixel dimensions for the current generation of focal plane arrays (FPAs) (less than 20 μm), or better, makes these techniques very attractive for identifying underlying causes of defects in the MCT epilayers.

Bulk investigations were performed by applying transmission x-ray diffraction techniques, such as white beam topography and rocking curves, which have already been used for the characterization of relatively thick CZT crystals.[3] Surface studies were performed using both synchrotron white beam x-ray topography (SWBXT) and rocking curves in reflection geometry. Fourier transform infrared (FTIR) microspectroscopy and infrared (IR) microscopy were performed as well to investigate IR transmission through the substrates. In fact, IR transparency (with good efficiency in the range of wavelengths of interest) of CZT substrates is important for the development of devices that use backside illumination.

EXPERIMENT

Five 1 mm thick $Cd_{1-x}Zn_xTe$ (x = 0.04) slices, four purchased from Nikko Materials (Tokyo, Japan) and one provided by Charles University (Prague, Czech Republic), were investigated. Three of them, measuring 20 mm × 20 mm, were previously characterized by Night Vision and Electronic Sensors Directorate (NVESD, Ft. Belvoir, VA) using a Bede D1 diffractometer (Durham, UK) with a sealed tube CuKα source and a four-circle goniometer (the beam was monochromated by a two bounce Ge channel cut crystal oriented to select the CuKα1 line). Measurements on the other two samples, measuring 10 mm × 10 mm, were performed for the first time.

SWBXT[4] was performed at the X19C beamline, which allows for a 40 mm × 5 mm maximum beam size in the energy range of 6–50 keV. SWBXT was used to image the (211)B surfaces (up to a depth of about 10 μm) of the substrate in reflection geometry to reveal the overall distribution of defects and any

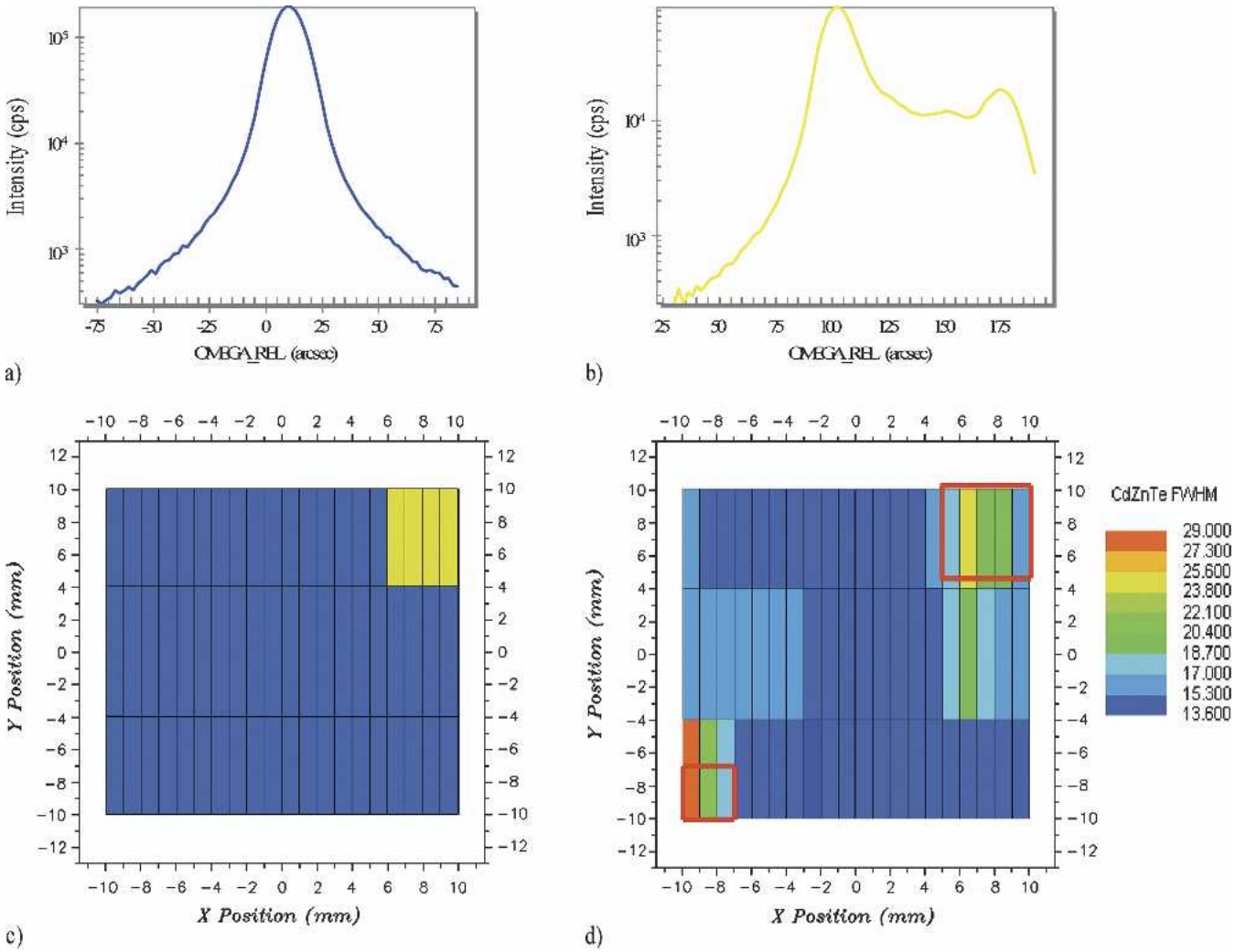

Fig. 1. Sample 5: Rocking curve mapping of the (244) reflection with a 0.5 mm × 8 mm x-ray beam and 1 mm (horizontal) and 8 mm (vertical) step size. Two typical shapes were identified: (a) single peak and (b) multiple resolved peaks. (c) This map associates the shape of the rocking curve with the location on the wafer. The colors correspond to the previous definition. (d) Map of FWHM values across the surface. For those areas shown in blue on the previous chart, the FWHM values shown here are for regions with a single peak. For those areas shown in yellow on the previous chart, the FWHM values shown here are for the highest intensity peak among multiple peaks.

distortion at the surface of the crystals. The (111) reflection was recorded in a single short exposure (8 s) on high-resolution x-ray films (Kodak Industries SR 45, Rochester, NY) with a spatial resolution approaching 1 μm (film grain size).

Transmission white beam x-ray topography (TWBXT) was performed at the X17B1 beam line with a 22 mm × 300 μm beam in the energy range of 50–200 keV. For this experiment, an image plate with a resolution of 50 μm was positioned at a sufficient distance from the sample to greatly reduce the background. Both the image plate and sample were translated simultaneously in the same direction with a synchronized movement. Large areas of the crystals were scanned to determine their bulk microstructures.

Each white beam x-ray topography (WBXT) image (topograph) was obtained by projecting the distribution of diffracted intensity produced by an area-filling x-ray beam incident on the sample onto a film or an image plate. The basic setups for both reflection (Bragg) and transmission (Laue) geometry are very simple, and they take advantage of the unique capability that synchrotron radiation (SR) offers in terms of a low-divergent, homogeneous, and bright beam. Short exposure times, between milliseconds and seconds, are required to record a white-beam topograph. Moreover, the small ratio between the source dimension and the source distance allows a high-resolution scan of the sample.

To complement these experiments, rocking curve maps were acquired in reflection and transmission geometry to study the surface and bulk crystal quality respectively. The X17B1 beam line was utilized to take advantage of a sagittal focusing double Laue monochromator,[5,6] which gives a highly collimated beam with a divergence of 10^{-5} rad and a flux of 10^{11} photons/sec. The availability of two stages, located at the center of the triple axis, allows x-y scanning of the crystal, thereby enabling a point-by-point

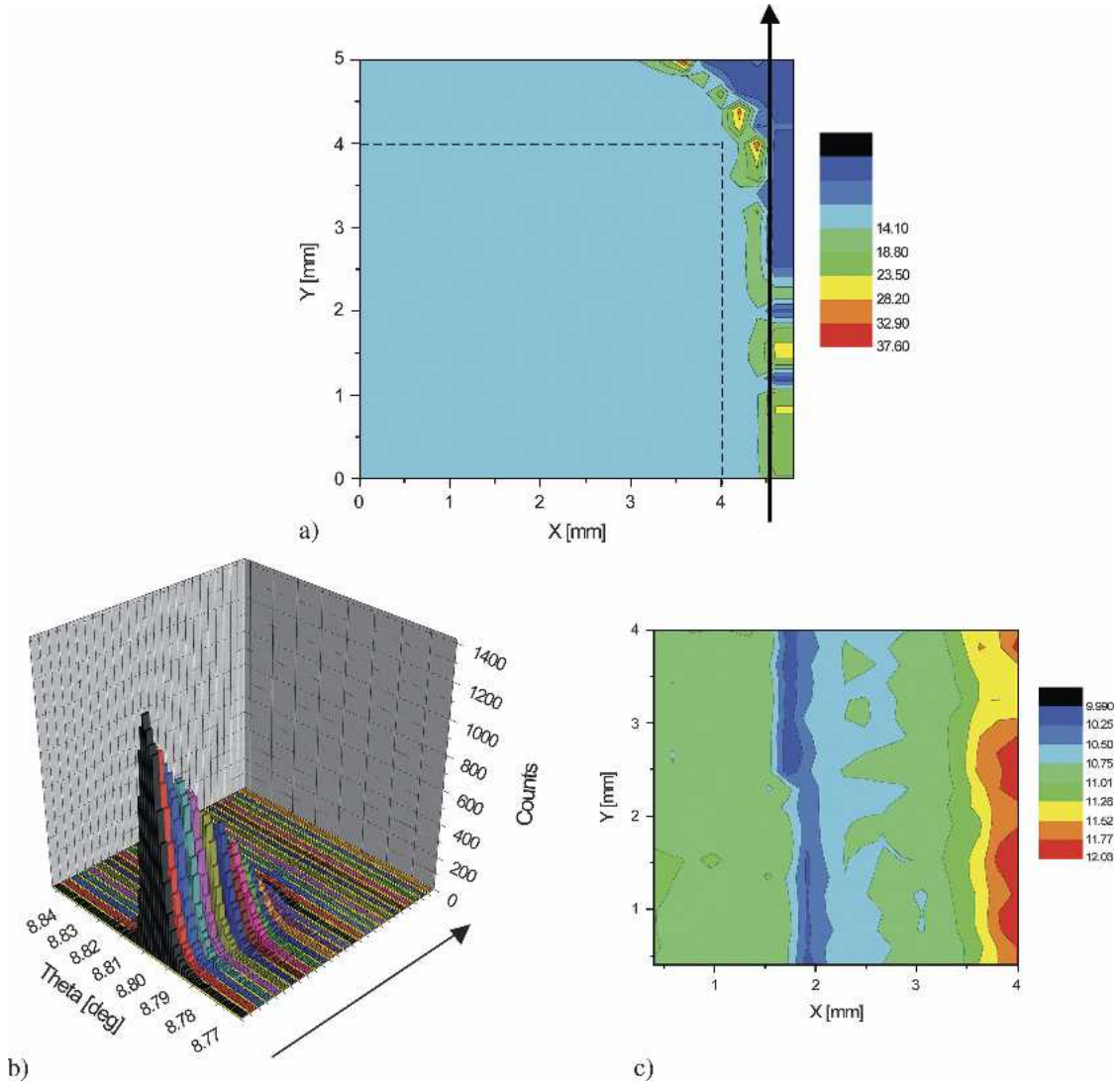

Fig. 2. Sample 5: Rocking curve mapping of (844) reflection with a 100 μm × 130 μm (over the sample), 67 keV beam, and a 200 μm step in both horizontal and vertical directions. (a) This map of FWHM values results from the measurements taken over the region corresponding to the yellow square at the top right corner in Fig. 1c. (b) Detail of the scan along the arrow drawn in map (a). (c) Mapping at a different scale shows smaller nonuniformities, which clearly follow the trend seen in the previous characterization [Fig. 1d].

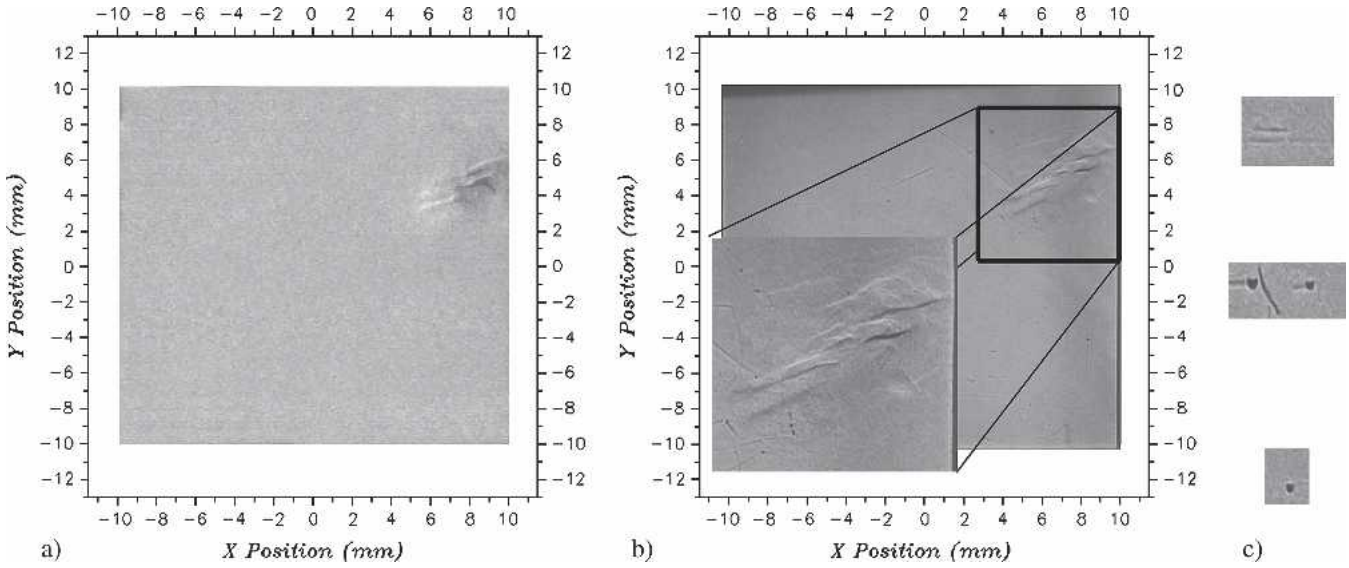

Fig. 3. Sample 5: (a) x-ray topograph, (224) reflection, acquired by the same step-and-measure technique used for rocking curves. The individual intensity images for every location on the wafer are then stitched together to form a topograph. Highly reflecting areas are bright on the image. (b) Synchrotron white beam x-ray reflection topograph (g = 111) recorded with a beam with energy ranges between 6 keV to 50 keV. (c) Te inclusion and trace details.

mapping. A 67 keV beam was used for the measurement. A 100 μm beam width and a typical step of 200 μm or 300 μm were used for both x and y steps. For each point of the raster scan, rocking curves were recorded through a detector positioned in a reflection direction at a location appropriate to achieve high sensitivity. The sample was finely rotated around an angle that meets the Bragg's condition, $\lambda = 2d_{hkl}\sin\theta_B$. Here, λ is the x-ray wavelength (0.185 Å/67 keV), d_{hkl} is the lattice plane spacing, and θ_B is the Bragg angle. This small angle variation makes it possible to record the angular distribution of the diffraction spot intensity without losing the reflection direction. A SPEC[7] macro (a UNIX based software package for instrument control and data acquisition developed for x-ray diffraction) controls the x-y stages, triple axis movements, and data acquisition system.

IR studies were performed using a Nicolet Magna-IR 560 FTIR spectroscope (Thermo Electron Corporation, Waltham, MA) to measure IR transmission spectra of the CZT substrates. A more complex investigation with a spatial resolution of 25 μm and 6.25 μm, at different depths of the samples, was possible with a Perkin-Elmer 300 FTIR spectrometer (Wellesley, MA).

RESULTS AND DISCUSSION

X-ray Diffraction Characterization

We first demonstrated the effectiveness of the characterization techniques at the [National Synchrotron Light Source (NSLS), Upton, NY] by investigating the crystal quality of a 20 mm × 20 mm substrate (sample 5) previously characterized at NVESD. Rocking curve mapping of the (244) reflection, with a 0.5 mm × 8 mm beam and 1 mm (horizontal) and 8 mm (vertical) step size, had identified rocking curves of two distinct shapes that were characteristic of distinct regions on the wafer (Fig. 1). We repeated the measurements in the area associated with the upper right-hand corner

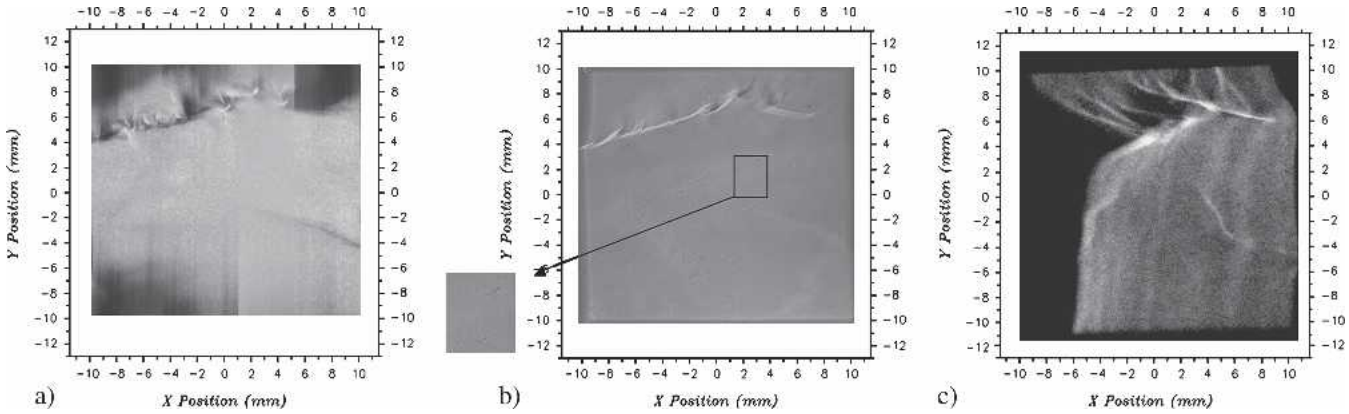

Fig. 4. Sample 4: (a) Topograph of (224) reflection acquired by the same step-and-measure technique used for rocking curves. (b) Synchrotron white beam x-ray reflection topograph (g = 111) along with a magnified section showing details of Te-inclusions and traces. (c) TWBXT topograph showing that the defects extend deep into the bulk of the crystal.

of the map in Fig. 1d. In this area, the rocking curves showed two peaks, each of which was broadened, for the (844) reflection with a 100 μm × 130 μm beam (over the sample) and a 200 μm step in both the horizontal and vertical directions. The results (Fig. 2) showed that the nonuniformities were localized at the edge of the sample. In this region the FWHM values range between 10 arc-sec and 14 arc-sec. In a second region (Fig. 1d, small red square in the left lower corner), the FWHM values have a smaller spread with an average of 10.5 arc-sec, and a small shift in the rocking curves peak positions was observed. These results validate that when a larger beam is chosen to perform a scan (e.g., to reduce the time required for this experiment) the resulting characterization suffers from loss in spatial precision with an associated loss in information pertaining to nonuniformities of the substrate properties.

Large area, high-resolution images of the sample were obtained by surface and transmission WBXT. The nonhomogeneous intensity distribution in the image (contrast) arising from distortion and strain fields enables visualization of structural defects and other material nonuniformities. SWBXT (Fig. 3b) revealed details of subgrain boundaries with misorientations on the order of 20–30 arc-sec, as well as inclusions (Fig. 3c) not identified in earlier characterizations. TWBXT confirmed the presence of the large boundaries, which extend deep into the crystal.

Surface topographs of the second 20 mm × 20 mm substrate (sample 4) corroborated the improvement in the visualization of small and extended defects as well (Fig. 4), while the transmission topograph depicted the extension of the grain boundaries visible at the surface into the bulk of the substrate.

The last 20 mm × 20 mm substrate (sample 3) broke along a line extending along a grain boundary (see discussion and figures in the next paragraph). Beside intensity undulations corresponding to strain field, the surface topograph of this sample exhibits interesting features such as clusters of dots, with a density greater than 300 cm^{-2} and sizes ranging from 10 μm to 60 μm in diameter. A line of closely spaced dots was also observed. Even though transmission characterization suffers from limited sensitivity to weak distortions, the transmission topograph of this crystal showed interesting similarities with other bulk investigations, as discussed below.

Rocking curve mapping of the two 10 mm × 10 mm samples was performed in transmission. Probing the (022) direction for the first substrate (sample 1), we observed several nonuniformities (Fig. 5a), including a region with a double peak rocking curve profile. The average FWHM value is around 8 arc-sec, increasing up to 15 arc-sec in a wide area of the crystal. The map of the second small substrate (sample 2) along the (333) direction indicated excellent quality (Fig. 5b) with an average FWHM value of almost 6 arc-sec. However, nonuniformities are present at the edges and broader FWHM values (up to 11 arc-sec) were observed at a corner. These scans were performed with a 100 μm × 100 μm beam size and a 300-μm step in both horizontal and vertical directions.

Surface topographs of both samples are almost uniform, revealing a good-quality surface with very few inclusions and a grain boundary of slight misorientation for sample 2. Transmission topographs exhibited features similar to other bulk investigations. Correlations for samples 1, 2, and 3 are described in the next paragraph.

IR Characterization and Data Correlation

IR transmission spectra were recorded from 6000 cm^{-1} to 400 cm^{-1} at a resolution of 4 cm^{-1} at room temperature. All samples showed IR transmittance between 63% and 67%, as expected for high-quality CZT samples (Fig. 6). The sample with the best crystalline quality also has the highest transmittance (sample 2). By analyzing data with respect to the transmittance values at the extremes of the range of interest, we can qualitatively determine the mechanism affecting the deterioration of the infrared transmittance and ultimately the defect structures responsible for the loss of transmittance.[8,9]

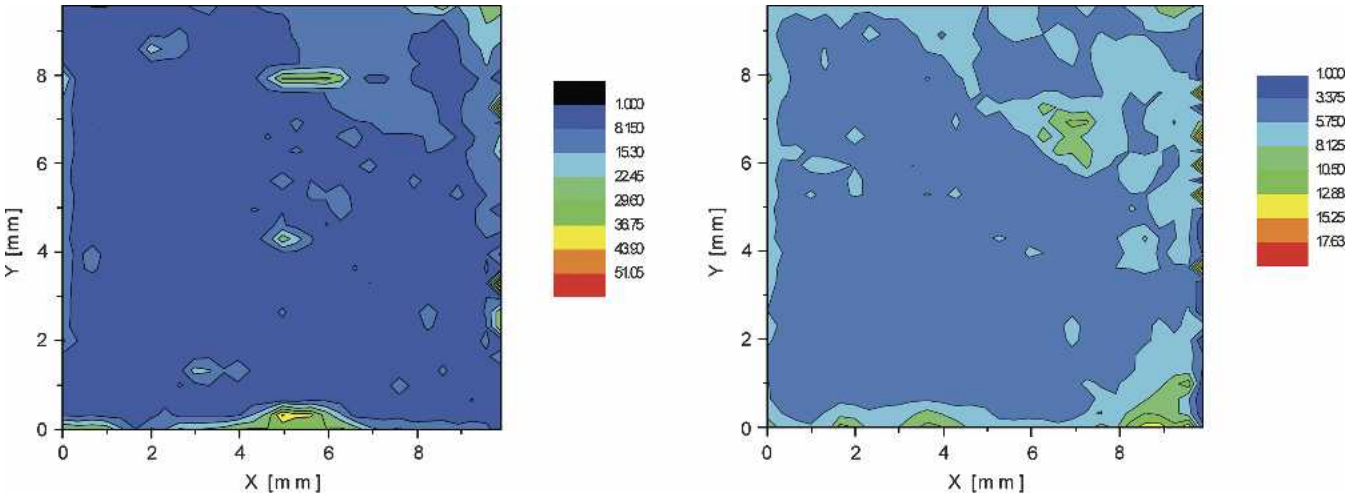

Fig. 5. Maps of FWHM values: (a) sample 1 and (b) sample 2. The "oval" area near the upper center of the maps correspond to a double peak Gaussian rocking curves region.

Two mechanisms are mainly responsible for transmittance reduction: scattering effect from Te-rich phases smaller than 1 μm[8] and free-carrier absorption. The free-carrier concentration changes with the concentration of point defects. Te-rich phases, subgrain boundaries, and dislocations may influence the point defect structure and result in free-carrier absorptionIR transmission spectra were recorded from 6000–400 cm^{-1} at a resolution of 4 cm^{-1} at room temperature (Fig. 6). The transmittance of the five samples varies from 63–67%, in the range of interest, as expected for high-quality CZT substrates. The sample with the best crystalline quality also has the highest transmittance. Analyzing these data looking at the transmittance values at the extremes of the range of interest, we can qualitatively evaluate which mechanism mainly affect the transmittance and ultimately the defect structures,[7,8] which reduces the IR transmittance of CZT. Scattering makes a significant contribution to the transmission of IR radiation with wavelengths smaller than 6 μm (i.e., wave numbers higher than 1667 cm^{-1}).[8] Thus, we can assume that for higher wavelengths the free-carrier absorption is chiefly responsible for the transmittance deterioration.

Figure 6 shows that samples 4 and 5 have almost the same type of spectra with transmittances of 63% and 65%, respectively; for sample 5, both free-carrier absorption and scattering provide a small contribution to the transmittance. Moreover, the substrate with higher transmittance also exhibited a better crystal quality, as observed for the samples discussed in the previous paragraph.

Sample 3 shows a significant deterioration related to the scattering whereas the spectra of samples 1 and 2, though different, exhibit slightly higher free-carrier absorption than that of sample 2.

Transmission FTIR scans of the five samples were also performed. In these maps, the total absorbance in the 720–7800 cm^{-1} wave number range is used as a parameter to reveal nonuniformities in a layer a few hundred microns thick below the surface of the sample. An interesting correlation with the TWXBT is observed. We first considered two regions of sample 3. Figure 7 illustrates the first region with the evolution of the line of closely spaced dots. This line, readily visible in SWXBT and on the transmission topograph, is revealed in greater detail on the FTIR map. FTIR scans from the second region (Fig. 8) show excellent correlation even for smaller features and clearly demonstrate the good resolution of FTIR maps.

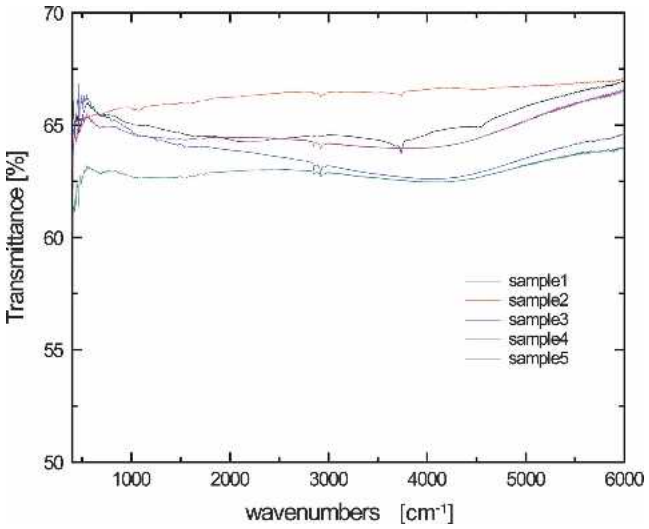

Fig. 6. Transmission IR spectra of the five substrates.

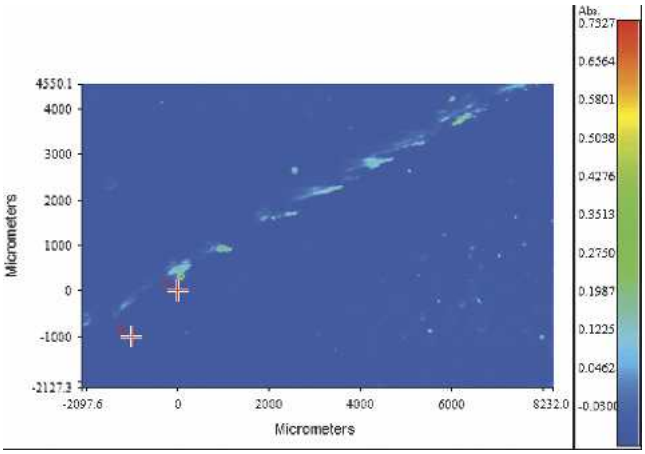

Fig. 7. Sample 3: FTIR microspectroscopy absorption map with 25 μm resolution.

Finally, sample 1 (Fig. 9a) manifested an interesting correspondence between a side region with higher IR absorbance and a lower transmission area in the topograph image. Smaller features seem to correlate in the case of sample 2 (Fig. 9b), where two corners show similar pseudo-circular shapes in both maps.

CONCLUSIONS

X-ray rocking curve maps and topographic images were acquired at NVESD using a conventional x-ray

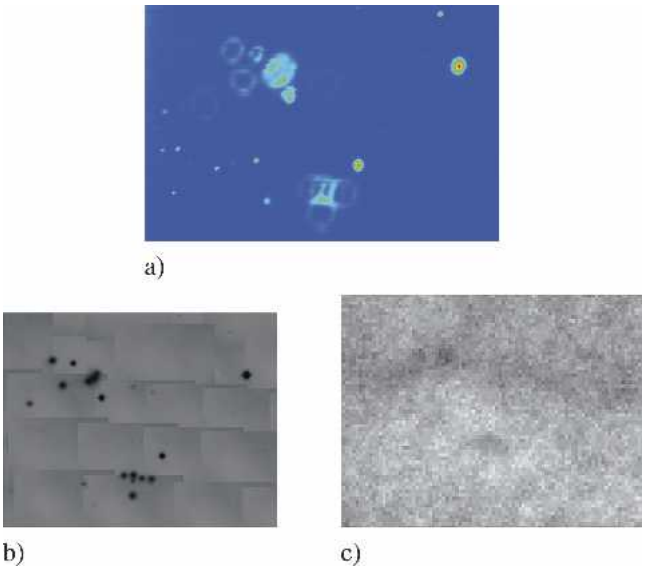

Fig. 8. Sample 3: correlation between characterizations performed with different techniques. (a) FTIR microspectroscopy absorption map with a 6.25-μm resolution. (b) Near IR-transmission map. (c) White beam diffraction topograph.

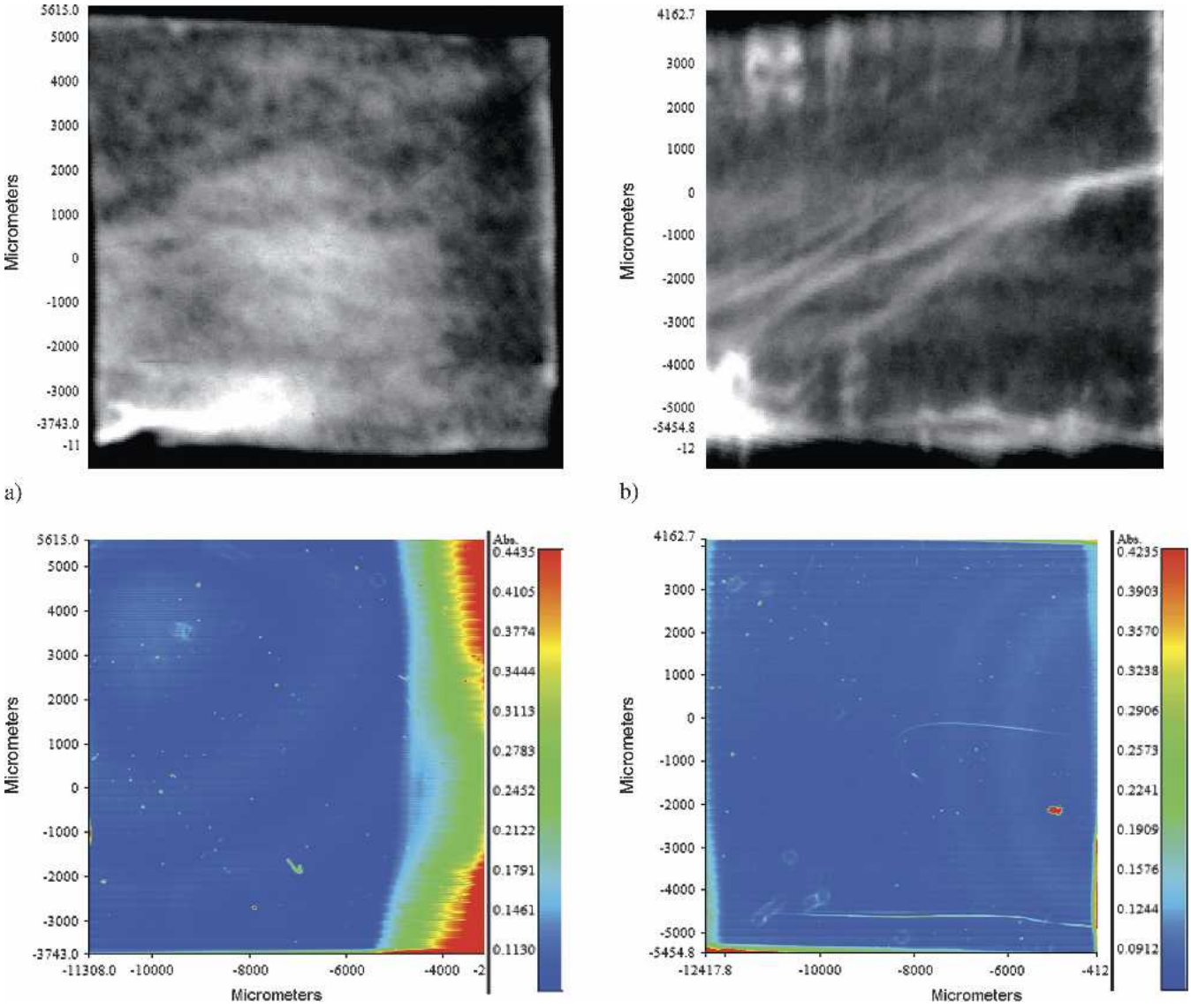

Fig. 9. Transmission x-ray topographs and FTIR transmission maps with a 25 μm resolution: (a) sample 1 and (b) sample 2. Pseudo-circular shapes in the left higher and lower corner correlate in both TWBXT and FTIR images.

diffraction apparatus and at NSLS using synchrotron radiation. The improved spatial resolution inherent in the synchrotron radiation is exploited to reveal defects in CZT wafers that are not well resolved in conventional topographs. In addition, the availability of transmission-mode techniques at NSLS leads to new information about defects throughout the bulk of the wafers. Application of x-ray and IR characterization techniques to study both bulk and surface properties yields a more detailed characterization of the CZT substrates than is available from a surface map only. Future work will include local compositional analysis and experiments to investigate correlations with epilayer properties.

ACKNOWLEDGEMENTS

The authors gratefully acknowledge the support of all the staff, technicians, and scientists of the National Synchrotron Light Source, particularly Pete Siddons, Lisa Miller, Larry Carr, Adele Wang, Michael Apple, and Jean Jakoncic. We wish to thank Jan Franc and Pavel Hoschl (Charles University, Prague) for providing one CZT substrate.

This manuscript has been authored by Brookhaven Science Associates, LLC under Contract No. DE-AC02-98CH1-886 with the United States Department of Energy. The United States Government retains, and the publisher, by accepting the article for publication, acknowledges, a worldwide license to publish or reproduce the published form of this manuscript, or allow others to do so, for the United States Government purposes.

REFERENCES

1. R.J. Koestner and H.F. Shaake, *J. Vac. Sci. Technol. A* 6, 2834 (1988).

2. J. Zhao et al., *J. Electron. Mater.* 33, 881 (2004).
3. G.A. Carini, G.S. Camarda, Z. Zhong, D.P. Siddons, A.E. Bolotnikov, G.W. Wright, B. Barber, C. Arnone, and R.B. James, *J. Electron. Mater.* 34, 804 (2005).
4. M. Dudley and X.R. Huang, *Encyclopedia of Materials: Science and Technology,* ed. K.H.J. Buschow, R.W. Cahn, M.C. Flemings, B. Ilschner, E.J. Kramer, and S. Mahajan (New York: Elsevier Science, 2001), pp. 9813–9825.
5. Z. Zhong, C.C. Kao, D.P. Siddons, and J.B. Hastings, *J. Appl. Crystallogr.* 34, 504 (2001).
6. Z. Zhong, C.C. Kao, D.P. Siddons, and J.B. Hastings, *J. Appl. Crystallogr.* 34, 646 (2001).
7. http://www.certif.com.
8. R.D.S. Yadava, B.S. Sundersheshu, M. Anandan, R.K. Bagai, and W.N. Borle, *J. Electron. Mater.* 23, 1349 (1994).
9. L. Yujie, G. Zhi, L. Guoqiang, and J. Wang, *J. Electron. Mater.* 33, 861 (2004).